

Flow and self-noise around bypass transition strips

Van Der Velden, W. C.P.; Van Zuijlen, A. H.; De Jong, A. T.; Ragni, D.

DOI

[10.3397/1/376559](https://doi.org/10.3397/1/376559)

Publication date

2017

Document Version

Final published version

Published in

Noise Control Engineering Journal

Citation (APA)

Van Der Velden, W. C. P., Van Zuijlen, A. H., De Jong, A. T., & Ragni, D. (2017). Flow and self-noise around bypass transition strips. *Noise Control Engineering Journal*, 65(5), 434-445. <https://doi.org/10.3397/1/376559>

Important note

To cite this publication, please use the final published version (if applicable). Please check the document version above.

Copyright

Other than for strictly personal use, it is not permitted to download, forward or distribute the text or part of it, without the consent of the author(s) and/or copyright holder(s), unless the work is under an open content license such as Creative Commons.

Takedown policy

Please contact us and provide details if you believe this document breaches copyrights. We will remove access to the work immediately and investigate your claim.

Flow and self-noise around bypass transition strips

W.C.P. van der Velden^{a)}, A.H. van Zuijlen^{a)}, A.T. de Jong^{a)} and D. Ragni^{a)}

(Received: 30 January 2017; Revised: 8 September 2017; Accepted: 13 September 2017)

To analyze the downstream effects of bypass transition strips on a laminar incoming flow, a direct numerical simulation of the fully transient, explicit and compressible Lattice Boltzmann equations is performed. Near wake analysis of a staggered grid of cubic blocks as transition device is compared with a more conventional zigzag strip, to ensure transition to a fully developed conical boundary layer. The staggered grid of blocks is more efficient in stopping the flow and creating large, coherent, flow structures of the size of the blocks, which results in a stronger transition. However, the downstream merging of spanwise created structures is relatively long resulting in higher correlated boundary layers. If the spanwise variation of the zigzag strip is small, the streamwise vortices created merge quicker, resulting in an earlier uncorrelated boundary layer. The self-noise created by zigzag strip is also significantly less than the noise from the staggered grid of blocks and becomes only dominant at high frequency compared to the predicted trailing edge noise. © 2017 Institute of Noise Control Engineering.

Primary subject classification: 21.6.4; Secondary subject classification: 75.3

1 NOMENCLATURE

δ	Local boundary layer thickness
δ_0	Incoming boundary layer thickness
δ_{ij}	Kronecker delta
δ_H	Displacement thickness
ν	Viscosity
Φ	Power spectrum or power spectral density
ρ	Density
τ	Relaxation time parameter
θ	Momentum thickness
ω	Weight functions
γ	Correlation coefficient
a	Speed of sound
b	Width, span
C_i	Bhatnagar–Gross–Krook collision term
c_i	Discrete velocity vector
f	Frequency
f_i	Movement of the distribution of particles function
H	Shape factor
k	Roughness height
l	Plate length
M	Mach number
p	Pressure
Re	Reynolds number
St	Strouhal number
t	Time
u_i	Velocity vector

x	Streamwise location
y	Wall normal location
y^+	Viscous grid spacing
z	Spanwise location

2 INTRODUCTION

To force the flow from a laminar state into a turbulent state at a specific position of interest, a boundary layer transition trip is generally used. As an additional effect, boundary layer transition often prevents laminar separation bubbles on airfoils from occurring, thereby reducing drag and improving the airfoil performance^{1,2}. During more recent applications, transition strips were used to match transition locations and boundary layer growth so that similar trailing edge flow characteristics were obtained when comparing, e.g., airfoil noise simulations with acoustical experiments. Although passive bypass transition offers a good solution to enforce transition, it is known that they will introduce disturbances which remain coherent far downstream, making it a challenge to have a fully conical turbulent boundary layer. In general, due to the large introduced disturbances by a tripping device, questions as: (1) which and what kind of flow structures are actually initiated by these passive devices, (2) how long do these structures persist downstream and (3) how do they develop into a fully developed turbulent boundary layer would be remain of crucial interest³.

Though the flow topology arising from the so-called bypass transition process⁴ is extensively addressed in the past, several issues are left open. Both experimental^{5–10},

^{a)} Delft University of Technology, Faculty of Aerospace Engineering, Aerodynamics Department, Kluyverweg 2, 2629 HT Delft, THE NETHERLANDS; email: W.C.P.vanderVelden@TUDelft.NL.

devoting to the description of the transition process by means of two-dimensional roughness strips, and numerical studies^{11–13}, describing the challenges with immersed boundary (IB) methods to represent the trip, have been conducted in the past. Previous attempts into the analysis of the flow topology included oil film surface flow visualizations and particle image velocimetry (PIV) behind a zigzag strip^{8,9}. The oil flow visualizations revealed backflow in small regions directly downstream of the upstream pointing spike, which are followed by clear oil stripes, indicating streamwise flow streaks. These streamwise streaks are confirmed by the PIV analysis as streamwise vortices and experience maximum spatial energy growth after which they develop into turbulence¹⁴. The spanwise vortical related structures directly behind the trip break up slowly into individual arches and start to develop into hairpin structures which are typical for wall turbulent bounded flows⁹. These elongated streaks of mostly low speed flow are a common feature in multiple bypass transition studies and unwanted since they promote coherence in the flow. They are present by either flows tripped by roughness as well as by free-stream turbulence^{15,16}. The far downstream effects of various trips are also investigated by, e.g., Erm and Joubert¹⁰. They showed that the influence of various trips far downstream of the trip disappears and that velocity statistics return to their common values for a fully developed turbulent boundary layer, which is a good effect for an uncorrelated boundary layer.

The motivation for the current research is to understand the properties of simulated transition strips for future aeroacoustic simulations. Particularly, the effect of boundary layers generated by these strips on trailing edge noise is interesting. The pressure and flow coherence downstream of a transition strip can influence the evaluation of trailing edge noise when the velocity statistics do not normalize in a sufficient downstream length. The study will compare different geometries and conclude on their effectiveness to generate a physical correct and uncorrelated boundary layer, focusing on the streamwise length it would take. Furthermore, the trip self-noise will be measured and compared with the prediction of the resulting trailing edge noise. This way, contamination of trip self-noise on trailing edge noise calculations can be predicted and better understood for future studies.

In recent years, an efficient and highly parallelizable approach for the simulation of fluid flows experiences increased attention in industry, known as the Lattice Boltzmann method (LBM)^{17–22}. The LBM solves the discrete Boltzmann equations in combination with a collision model to compute the flow of a Newtonian fluid. By modeling the convection and collision processes of a limited number of particles, the flow is represented on a macroscopic scale. The LBM methodology is used in the

present study to analyze the low Mach number fluid flow around a zigzag trip and a staggered grid of cubic cubes.

3 METHODOLOGY

The commercial software PowerFLOW 5.0b is used to compute the flow field. The software solves the discrete Lattice Boltzmann (LB) equations for a finite number of directions. For a detailed discussion, the reader can refer to Succì²³. The LB method determines the macroscopic flow variables starting from the mesoscopic kinetic equation, i.e., the LB equation. The discretization used for this particular application consists of 19 discrete velocities in three dimensions (D3Q19), involving a third-order truncation of the Chapman-Enskog expansion. It was shown that this scheme accurately approximates the Navier-Stokes equations for a perfect gas at low Mach number in isothermal conditions²⁴. The distribution of particles is solved by the mean of the LB equation on a Cartesian mesh, known as a lattice. An explicit time integration and a collision model are used. The LB equation can then be written as follows:

$$g_i(\mathbf{x} + \mathbf{c}_i \Delta t, t + \Delta t) - g_i(\mathbf{x}, t) = C_i(\mathbf{x}, t), \quad (1)$$

where g_i is the particle distribution function. It statistically describes the particle motion at a position \mathbf{x} with a discrete velocity \mathbf{c}_i in the i direction at time t . $\mathbf{c}_i \Delta t$ and Δt are space and time increments, respectively. $C_i(\mathbf{x}, t)$ is the collision term; the Bhatnagar–Gross–Krook (BGK) model^{24,25} is adopted because of its simplicity:

$$C_i(\mathbf{x}, t) = -\frac{\Delta t}{\tau} \left[g_i(\mathbf{x}, t) - g_i^{eq}(\mathbf{x}, t) \right], \quad (2)$$

where τ is the relaxation time and g_i^{eq} is the local equilibrium distribution function. For small Mach number flow, the equilibrium distribution of Maxwell-Boltzmann is conventionally used²⁴. It is approximated by a 2nd order expansion as:

$$g_i^{eq}(\mathbf{x}, t) = \rho \omega_i \left[1 + \frac{\mathbf{c}_i \mathbf{u}}{c_s^2} + \frac{(\mathbf{c}_i \mathbf{u})^2}{2c_s^4} + \frac{|\mathbf{u}|^2}{2c_s^2} \right], \quad (3)$$

where ω_i is the fixed weight functions, dependent on the velocity discretization model D3Q19²⁴, and $c_s = 1/\sqrt{3}$ is the non-dimensional speed of sound in lattice units. The g_i function is related to the macroscopic quantities density ρ and velocity \mathbf{u} as:

$$\rho(\mathbf{x}, t) = \sum_i g_i(\mathbf{x}, t), \quad \rho \mathbf{u}(\mathbf{x}, t) = \sum_i \mathbf{c}_i g_i(\mathbf{x}, t). \quad (4)$$

The dimensionless kinematic viscosity (ν) is related to the relaxation time following Chen²⁴:

$$v = c_s^2 \left(\tau - \frac{\Delta t}{2} \right). \quad (5)$$

A direct simulation of the LBM relations is employed. A variable resolution is allowed, where the grid size changes by a factor of two for adjacent resolution regions. Due to the explicit time-stepping characteristics of the LBM scheme, the time-step size is increased with cell size in factors of two as well. Larger cells will therefore not be evaluated every time-step. This gives rise to the notation of time-step equivalent number of cells, which is the number of cells scaled to operation at the shortest time-step in addition to the total number of cells.

4 CASE SETUP

The flow topology around two transition strips, the upper part of a $l = 350$ mm long and $0.0857l$ wide flat plate, is simulated. The tripping, seen in Fig. 1, is applied by either a staggered grid of blocks or zigzag strip of 2 mm thickness. The small cubic blocks of 2 mm each are 6 mm located away from each cubic center. In total, 4 rows of blocks are placed in a staggered grid at 9% of the flat plates chord. The second trip, a 9 times V-shaped zigzag strip of 5.5 mm length is also applied at 9% of the flat plate chord. Both trips (if considering every row of blocks) have a similar frontal area exposed to the fluid flow.

The simulation domain is bounded by a no-slip boundary condition at the location of the plate and by a frictionless wall at a $0.1l$ distance in wall-normal direction, making sure the distance does not interfere with the developed boundary layer. At the inlet, a streamwise velocity of 45 m/s is prescribed to run simulations at a chord based Reynolds number of 1.5×10^5 , the maximum which could be reached within a turn-around time of 15 days for 0.1

physical second of computational time on a system of 80 cores of Intel Xeon X5670 (hex-core) platform at 2.93 GHz. The outlet is modeled by fixing the static pressure, while maintaining a free flow direction. The LBM scheme is discretized over lattices of different sizes. The finest lattices of 32 cells per millimeter are positioned near the wall and at a larger area around the trip, including a wake refinement making it a direct, wall resolved, simulation. The viscous grid spacing ($x^+ = y^+ = z^+$) is directly extracted from the downstream friction velocity and equals 0.4. The DNS simulation in Exa PowerFLOW allows us to solve the boundary layer at a dense mesh, while outside the boundary layer, the mesh coarsens. In total, seven volumes of refinement (VRs) are used as indicated in Fig. 2, resulting in a total of 666 million voxels or 438 million fine equivalent voxels.

The experimental Mach number is about 0.13, but in the simulation, the Mach number has been increased to 0.31 in order to obtain a proper DNS resolution in all the refinement regions. When converting the physical quantities into dimensionless lattice quantities, the velocity is increased by approximately a factor of three while keeping the Reynolds number constant by increasing viscosity. After the computations, the data is converted back to the experimental values. The Courant–Friedrichs–Lewy (CFL) stability number is intrinsically set to unity by the solver, leading to a time step of 1.3×10^{-7} s, assuming a maximum velocity of 1.3 the freestream velocity. In physical time, the simulations are run for 0.3 s, where the last 0.25 s (i.e., 32 flow-passes) are used for recording statistics at a frequency of 30 kHz. Spectra are obtained using a Hanning window with 50% overlap, 22,000 frames with a FFT window width of 5400, resulting in an optimal smoothing.

The physical quantities from the LBM solution like velocities, pressures, and distances are made dimensionless in the next section using the free-stream velocity ($u_\infty = 45$ m/s) and the atmospheric pressure (p_∞) as well as the undisturbed laminar boundary layer thickness, δ_0 , which will be determined at the location where the trip starts ($x_0 = 0.09c$). If the thickness is determined using a Blasius profile, it results in:

$$\delta_0 = 5.0 \frac{x_0}{\sqrt{Re_{x_0}}}, \quad Re_{x_0} = \frac{u_\infty x_0}{\nu_\infty}, \quad (6)$$

which results in a Reynolds number of 1.4×10^4 and thickness of $\delta_0 = 1.4$ mm for the current setup. The undisturbed Reynolds number of the laminar boundary layer, Re_{θ_0} , is estimated to be 80 which is far below the thresholds of a transitional and turbulent boundary layer given by Preston²⁶ (i.e., $Re_{\theta_0} = 162$ and 320, respectively). This implies the usage of an imposed tripping device to bypass the transition process to provide a large disturbance and an added momentum loss.

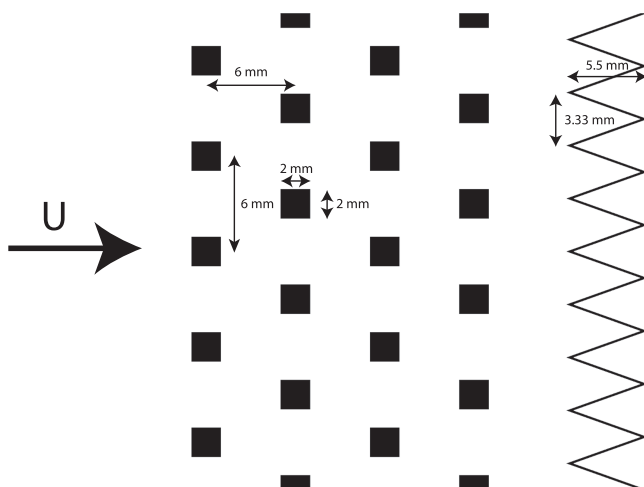


Fig. 1—Schematic view of both bypass transition devices; (left) the staggered grid of cubes and (right) the zigzag strip.

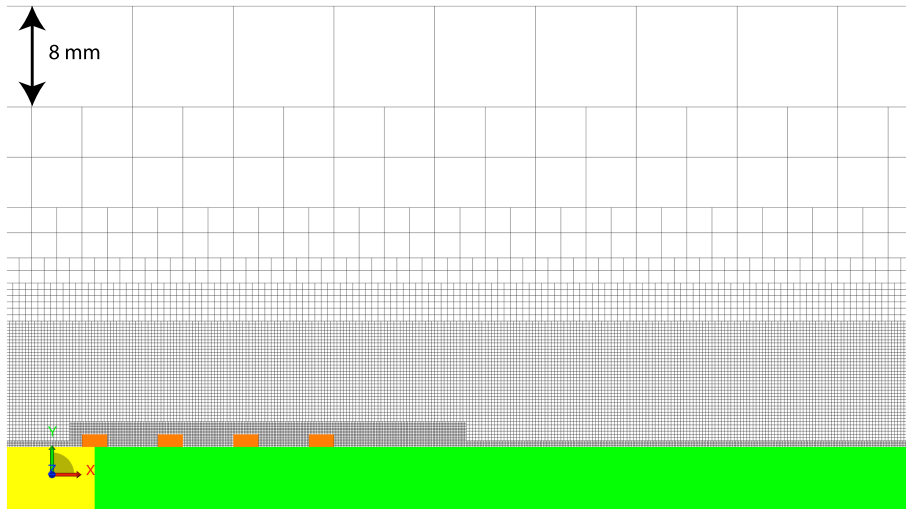


Fig. 2—Detailed view of the VR's near the block trip. Similar refinement regions are used for the zigzag strip model.

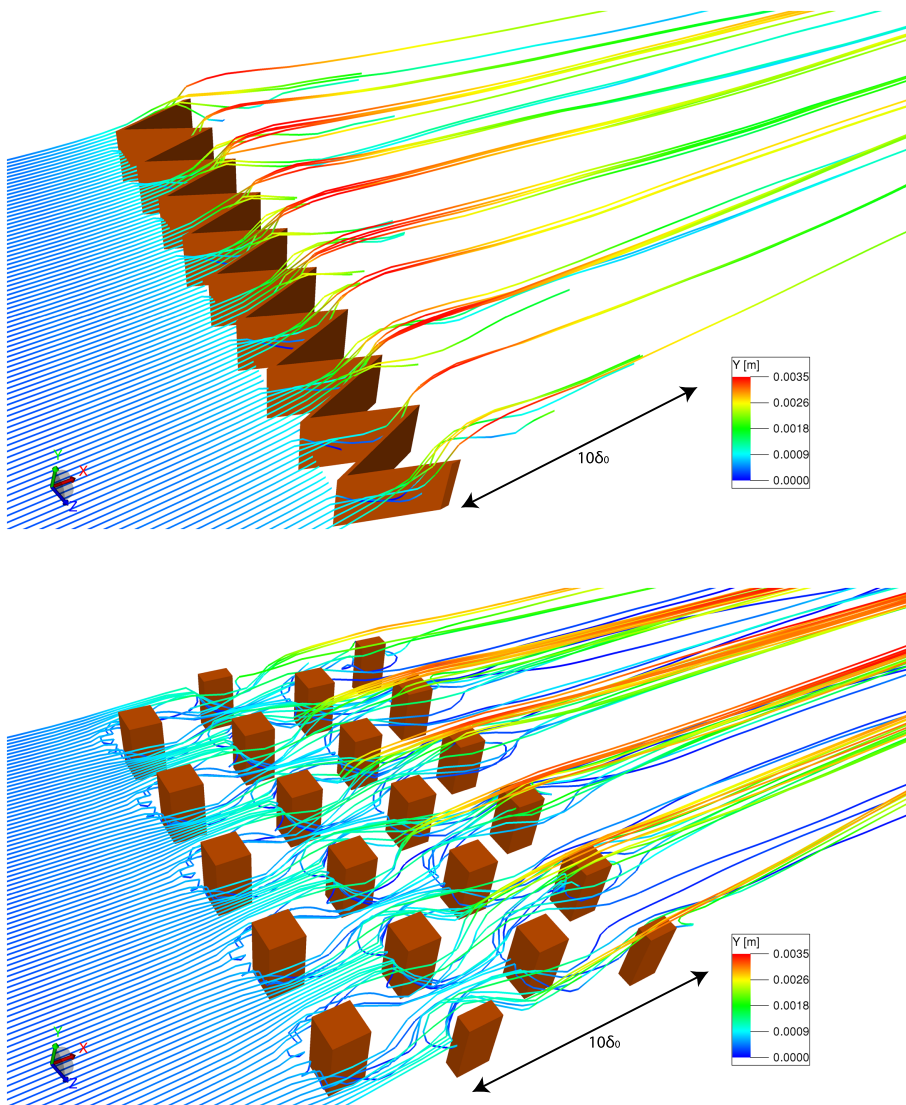


Fig. 3—Streamwise colored by wall-normal height illustrating the mean flow topology of the bypass transition behind the zigzag strip (top) and staggered grid of blocks (bottom).

The optimum trip height can be compared against some engineering tools for forcing a boundary layer available in literature from both Braslow and Knox,² and Gibbings²⁷. The minimum roughness height k_{cr} is determined based on the roughness height Reynolds number Re_k , which is obtained by extensive wind tunnel research. For two-dimensional tripping devices, Braslow and Knox,² and Gibbings²⁷ predicted a Reynolds number of $Re_k = 300$ and 850 , respectively, leading to a roughness height of $k_{cr} = 0.7$ mm and 2.0 mm, respectively. van Rooij and Timmer¹ suggested on the other hand that, when three-dimensional trips are applied, the Reynolds number is reduced to $Re_k = 200$. This would imply a trip thickness of 0.5 mm. The large discrepancy between the values is illustrative for the differences in the results of aforementioned studies. It can be seen that the current test case ($Re_k = 800$) is slightly over-tripped, based on the other studies presented before.

5 RESULTS AND DISCUSSION

5.1 Bypass Transition Process

The three-dimensionality of the mean flow is analyzed using figures of streamlines around both bypass transitions strips, colored by their wall normal height. The results in Fig. 3 show a uniform flow before it is disrupted by the bypass transition strip. Clearly, for both trips, spanwise periodicity and symmetry are found back in the figure by means of compressed bundle of streamlines behind the

trip. The staggered grid of blocks seems to disturb the incoming flow less; flow is either moved around blocks (blue streamlines at the second and third row, see legend Fig. 3) or flows over a block (red streamlines at the last row) instead of stagnation appear at the entire frontal surface of the zigzag strip. The vortices created by the first rows are pushing the low-speed and back flow fluid away from the wall resulting in the higher speed fluid streaks over the last row. In the case of the zigzag strip, the incoming laminar boundary layer encounters a larger initial frontal area which covers the entire span. This enhances a wedge of continuous turbulence behind the trip, resulting in larger friction forces. Because of these additional disturbances in the flow, momentum drag is added, after which transition occurs²⁸. The streamlines reach their highest point directly after the downstream tip after which the high speed fluid is moved in the direction of the wall again. The overall drag is measured to be four times larger with a zigzag strip when comparing with the first row of blocks. The average drag coefficient is similar though if all rows of blocks are taken into account, with the first row contributing the most.

The results for the different velocity components are displayed in a wall-parallel plane in Figs. 4 and 5. For the zigzag strip, streak-like structures are present directly behind the trip, which extends at least $10\delta_0$. This is a common trend and observed in, for example, the study from Elsinga and Westerweel⁹. One thing though to observe in Fig. 4 is that, by applying the staggered grid of blocks

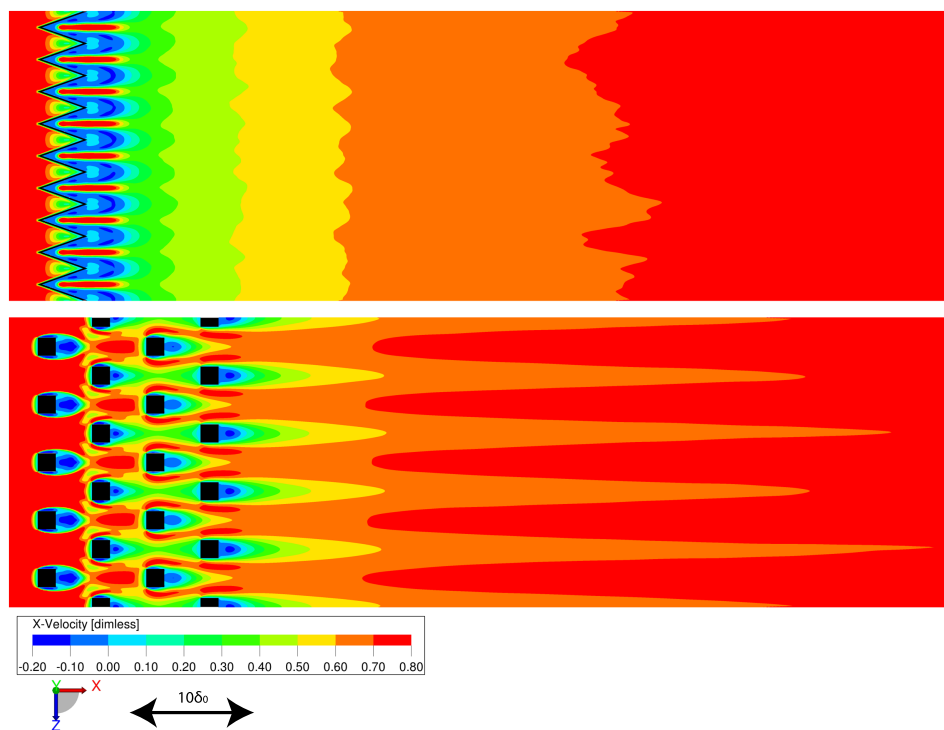


Fig. 4—Mean streamwise velocity behind the zigzag strip (top) and staggered grid of blocks (bottom) in a plane parallel to the wall at $y/\delta_0 = 1$.

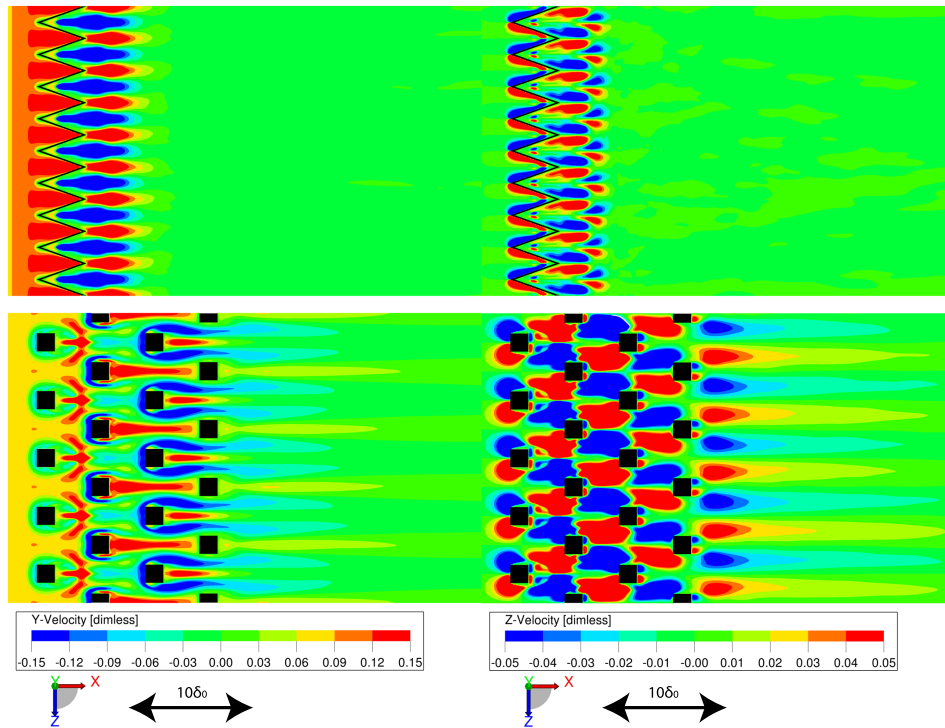


Fig. 5—Mean wall-normal (left) and spanwise (right) velocity behind the zigzag strip (top) and staggered grid of blocks (bottom) in a plane parallel to the wall at $y/\delta_0 = 1$.

as a bypass transition device, this results in a clearly less effective merging of the lower speed streaks. Visible streaks are present up to $80\delta_0$.

For the staggered grid of blocks, back flow is observed behind every single block which is made visible by the negative streamwise velocity component in the figure. The size of the backflow is a variable for each row of blocks, where the largest backflow can be seen in the first row. This backflow gradually decreases per row of block due to the increased drag of the blocks, resulting in a lower convective velocity. Less energetic boundary layer profiles (see Reynolds stresses in Figs. 6 and 7) hits the next row of blocks while energy transfer takes place vertically in the boundary layer. Similar conditions are found back in applications, e.g., energy extraction from a row of aligned wind turbines. Numerical studies, such as the modeling of rows of actuator disks, have been performed in the past²⁹. Furthermore, the flow moves towards the wall before a block appears and away from the wall behind a block. This wall-normal movement (denoted by negative velocities in Fig. 5) is the strongest behind the second row of blocks, where it appears as a long streak of upward moving fluid flow. The interaction of the first row and second row also results in flow moving away from the wall while the interaction between the second and third row creates flow structures being pushed towards the wall (see also Fig. 3). The spanwise velocity component alters (positive and negative) as expected around a single block, creating a diverging and converging pattern around the staggered grid. Behind the

last row of blocks, the non-uniformity stays for about $20\delta_0$, which could indicate periodical rows of packages of horseshoe vortices, to be confirmed in a later stage.

For the zigzag strip, uncorrelated flow features with minor streamwise, wall-normal and spanwise variations are observed earlier than by using a staggered grid of blocks (within $5\delta_0$). Directly behind the trip, the streaks are visible and backflow is observed together with a flow going away from the wall (as seen by the red streaks in the wall-normal velocity plot from Fig. 5). This behavior starts behind a downstream pointing tip of the zigzag strip. The upstream pointing tip on the other hand shows a region with positive but relatively small streamwise velocity ($u > 0$) with flow pointing towards the wall ($v < 0$). The spanwise component (Fig. 5) is clearly smaller using a zigzag strip compared to using a staggered grid of blocks. However, close to the downstream pointing tip, an altering pattern is present for the zigzag case. Positive oriented vortices (red and pointing down) are canceled and merged with negative orientated vortices (blue and pointing upwards) at the tip at a downstream location of the trip, enhancing the mixing which is useful for smaller and quicker recovery¹⁰. After the initial region with streaks, a region follows where the average flow regains its spanwise uniformity, merges and further accelerates in streamwise direction and is slightly directed towards the wall. This region covers approximately $10\delta_0$ (see Fig. 4), where after little variations are seen for the streamwise direction. This is expected for a fully developed turbulent boundary layer^{14,30}.

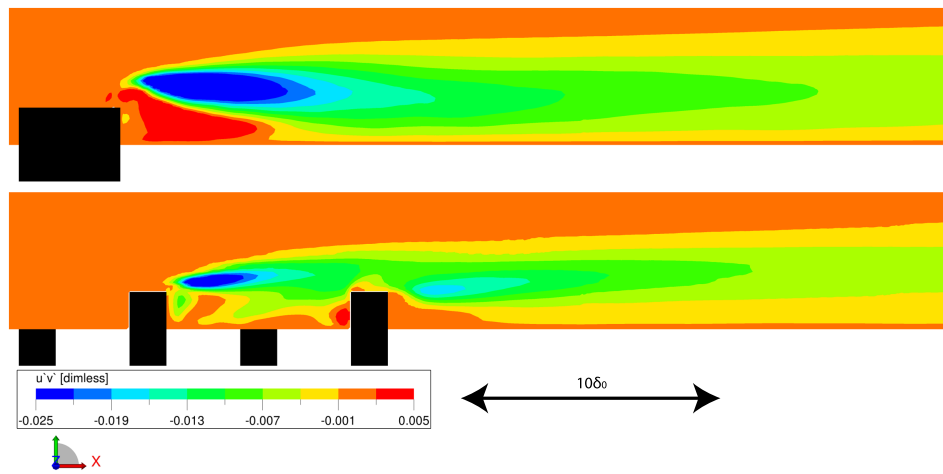


Fig. 6—Reynolds shear stresses of streamwise, wall-normal direction in a streamwise–wall-normal plane behind the zigzag strip (top) and staggered grid of blocks (bottom).

In Fig. 8, iso-surfaces of Λ_2 colored by velocity magnitude (low speed blue, high speed red) illustrate the instantaneous flow topology around the bypass transition process, with a limited domain width in streamwise direction. The general trend due to the three-dimensional nature of the trip shows a shear layer in which vortices roll up into spanwise coherent structures. These spanwise structures break up into individual arches that remain aligned according to the periodic nature of the trip. In both trip cases, the arches are inclined at about 45 degrees with the wall, which can be associated with increasing wall-normal fluctuations, which were already observed in $u'v'$ fluctuations in the previous section. This roll-up and orientation have been described by Ghaemi and Scarano³¹ before. Further downstream, the arches are merged with low speed quasi streamwise vortices (blue and green structures), resulting in the formation of hairpin like structures³². These legs become stretched because of the acceleration of the flow after the trip (Fig. 4) and rotate corresponding to their

spanwise and wall-normal variations. These hairpin-like structures form packages after which they convect and dissipate further downstream^{9,31}.

A difference between the staggered grid of cubic blocks and the zigzag strip is the spanwise merging of horseshoe vortices. The staggered grid enhances the effect of streaks of packages with hairpins, whereas the short spanwise wavelength between the arches of the zigzag strip enhances the merging process, so that, further downstream, no streamwise elongated streaks are present. This observation was already confirmed using Figs. 4 and 5.

The Reynolds spanwise normal stresses ($w'w'$) and shear stresses ($u'v'$) are presented in a streamwise–wall-normal plane through the last row of blocks and a downstream pointing tip for the staggered grid of blocks and zigzag strip respectively (see Figs. 6 and 7). The Reynolds stresses presented are about 5 times higher downstream than those in a general canonical developed turbulent boundary layer presented by, e.g., Klebanoff et al.³³, which

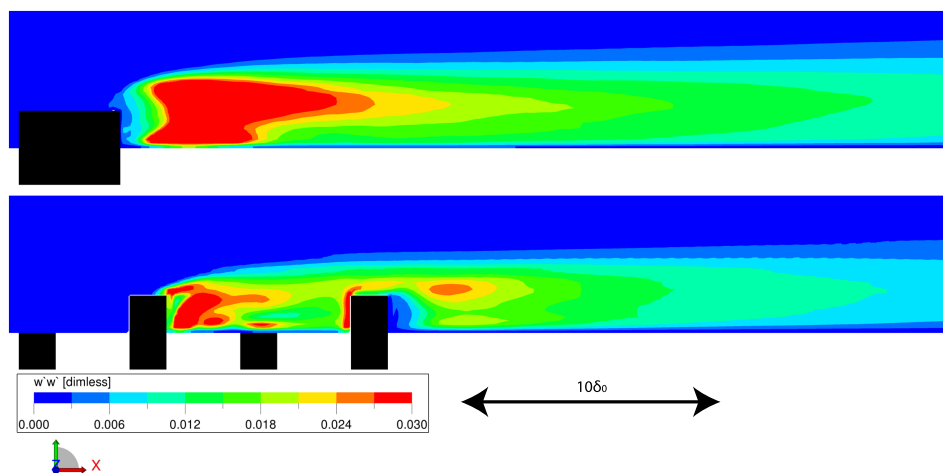


Fig. 7—Reynolds normal stresses in spanwise direction in a streamwise–wall-normal plane behind the zigzag strip (top) and staggered grid of blocks (bottom).

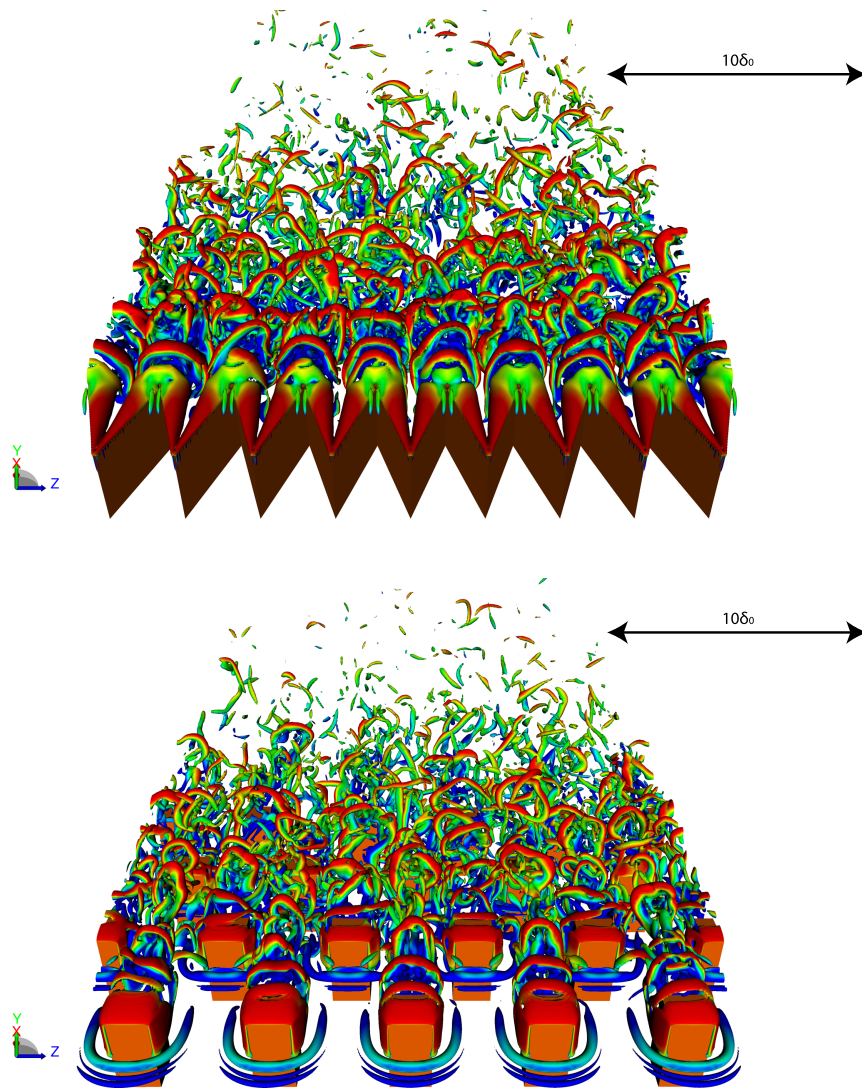


Fig. 8—Iso-surface of Λ_2 colored by velocity magnitude illustrating the instantaneous flow topology of the bypass transition behind the zigzag strip (top) and staggered grid of blocks (bottom).

are $w'w' = 1.6 \times 10^{-3}$ and $u'v' = -0.8 \times 10^{-3}$. However, the order of magnitudes is similar to other more recent studies behind turbulent transition^{9,34,35}. This would imply that at least the current measurement domain shown in the figures (approximately $80\delta_0$) remains affected by trip.

Both shear stress plots ($u'v'$) show the occurrence of a shear layer emanating from the trailing edge of either a block or zigzag strip. The trailing edge of the trip separates the reversed flow near the wall from the higher speed streaks in the outer flow. In the velocity plot, this introduced an inflection point which is a clear source of the generation of turbulence. For the staggered grid of cubic blocks, the thickness of the layer is influenced by the next row of blocks as can be seen from Fig 6. The flow is compressed and pushed upwards by the individual blocks, resulting in a less thick shear layer compared to the results from the zigzag strip.

The spanwise normal stress levels ($w'w'$ in Fig. 7) are larger close to the wall behind the separation compared

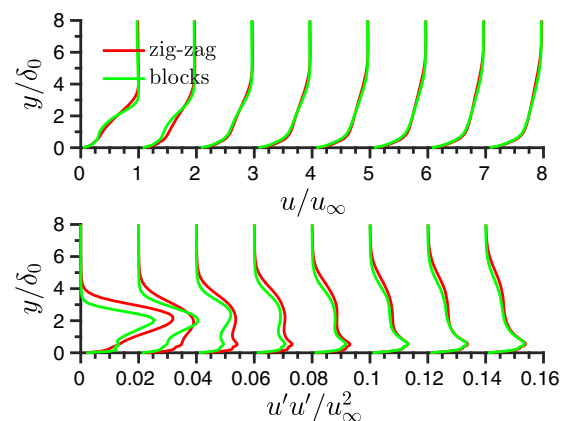


Fig. 9—Line plots of the downstream development of the boundary layer. Mean streamwise velocity (top) and Reynolds normal stresses (bottom), separated by $10\delta_0$.

to the trends found in shear stress levels. Behind the zigzag strip, the spanwise normal stress levels attain higher values compared to the other tripping mechanism. This is an indication for enhanced mixing towards a homogeneous turbulent boundary layer. This result is also in agreement with Fig. 5, where the breakup of spanwise structures is superior for a zigzag strip compared to a staggered grid of cubic blocks.

5.2 Downstream Development of the Boundary Layer

The downstream development of the Reynolds stresses suggests the proper transition towards a fully developed boundary layer. To confirm this result, line plots at $10\delta_0$ till $80\delta_0$ are plotted in Fig 9, showing both mean streamwise velocity and Reynolds normal stresses. The mean flow seems to be heavily affected by both transition strips within a $20\delta_0$ downstream distance. On the other hand, the normal stresses seem to take at least $60\delta_0$ to recover the flow. The zigzag strip shows a slightly larger boundary layer, as already concluded in Fig 6. In both bypass transitions, the shear layer thickness increases downstream and remains at approximately the same height, while the average flow reattaches and a transition to the turbulent regime is observed. The indication of high local shear flow indicates the transport of energy from near the wall fluid towards the higher momentum-fluid available in the flow. This effectively results in re-energizing the boundary layers.

To further investigate the recovery of the boundary layer, the shape factor at the same planes as before is extracted and plotted in Fig. 10. While the staggered grid of blocks attains slightly higher values close to the trip, both strips converge to a shape factor of $H = 1.5$. Clearly, the zigzag strip reaches this threshold earlier, at around $40\delta_0$, while the staggered grid of blocks needs to double the downstream distance to convergence.

To further analyze the development of the boundary layer, an instantaneous view of the spanwise vorticity is plotted in Fig. 11. Spanwise vortices are present over the entire computational domain, but the largest, locally bundled,

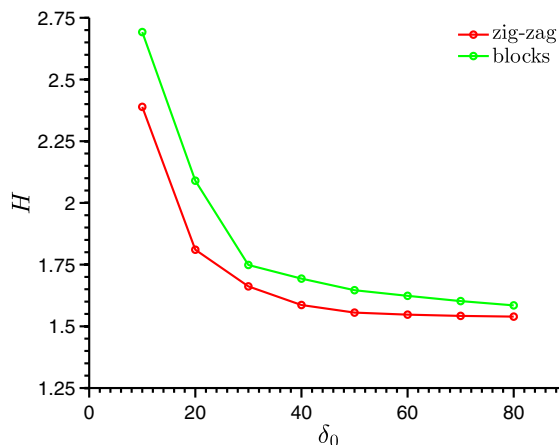


Fig. 10—Development of shape factor downstream the transition strip.

spanwise vortices are present until $10\delta_0$ downstream the zigzag strip, emphasizing the effective merging process of the hairpin like vortices. The staggered grid of blocks on the other hand only shows a minor increase in spanwise vorticity directly downstream the last row of blocks (Fig. 8). It is thought that the spanwise wavelength of both trips will play an important role in this merging effect, in order to speed up the development of the boundary layer.

The visualization of the vortical structures as well as the mean velocity plots implies that the spanwise periodicity of arches gradually disappears downstream. While vortical structures as horseshoes, arches and low speed streaks keep present in the flow, the initial structures from the tripping bring in an important spanwise coherence to the flow. To investigate the spanwise coherence, the auto spanwise correlation of wall pressure fluctuations is analyzed downstream the trips (Fig. 12).

The resulting profiles for the staggered grid of blocks show less of a decay compared to the zigzag trip results at the three downstream locations behind the trip. The zigzag strip on the other hand shows some dominating spanwise oscillations corresponding to the strong streaks behind the downstream pointing tips. The height of the correlation peaks drops quickly when going downstream, while

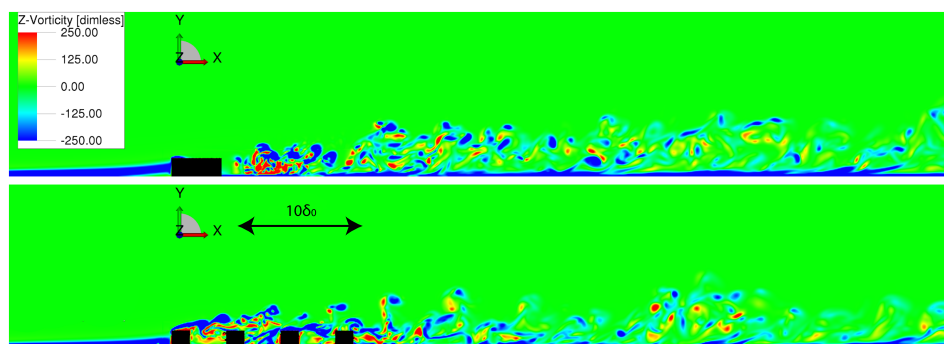


Fig. 11—Instantaneous spanwise vorticity behind the zigzag strip (top) and staggered grid of blocks (bottom) in a plane at mid-span.

a constant plateau around 0.0 is maintained at $40\delta_0$ spanwise distance. The staggered grid of blocks however shows a constant plateau around 0.075, which is strong evidence that large spanwise coherence structures remain present at downstream locations.

5.3 Acoustic Near-field Emission

Before investigating and comparing the direct acoustic effects of both trips, it has to be confirmed that both the downstream turbulent boundary layers have a similar energy spectrum. Therefore, in Fig. 13, the power spectral density of wall pressure is plotted. The results are obtained using a discrete fast Fourier transformation with a 50% Hanning window, sampled at a frequency of 30 kHz. Goody semi-empirical model³⁶ is attached for further comparison, and shows in general a good agreement with the obtained wall pressure spectrum from the LBM simulation. The match between both blocks and zigzag configuration is excellent, giving confidence of similar turbulent boundary layer noise emissions in the computational domain.

The final step is to analyze the near acoustic field. Due to the compressible nature of the LBM code, acoustics can directly be obtained in the undisturbed mean flow field. Pressure fluctuations have been sampled at a location of 0.11 above the centers of both trips and converted into frequency domain. Results are found in Fig. 14. Interestingly, a clear difference between the noise emission of the blocks and zigzag strip is observed. While at low frequencies, an increase of noise levels of about 5 dB for the blocks is found, an increase over 20 dB is found for higher frequencies.

Especially the high frequencies are of interest for this particular study, as trip noise tends to become dominant when the main noise source, e.g., trailing edge noise, becomes very small²². To confirm this, the surface pressure spectra discussed earlier in Fig. 13 are taken as input for the

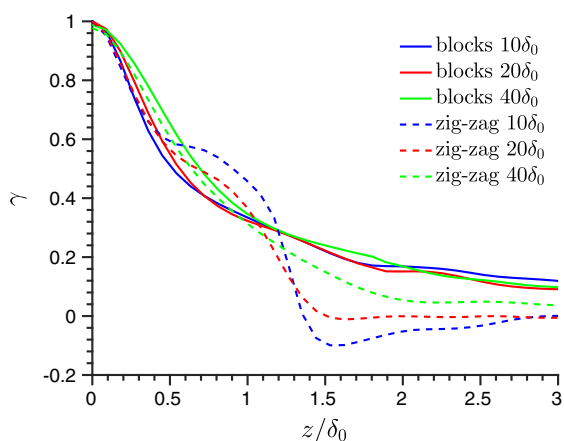


Fig. 12—Wall pressure spanwise cross-correlation at different planes behind the transition strip.

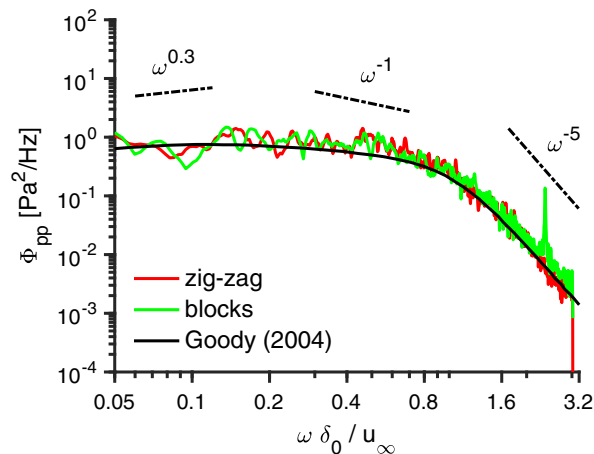


Fig. 13—Wall pressure fluctuations at last stage of measurement domain.

analytical prediction of trailing edge noise, by making use of the backscattering method of Moreau and Roger³⁷. It is found that, after $\omega\delta_0/u_\infty = 0.8$, the self-noise from the staggered grid of blocks is becoming the dominant noise source. Similarly, for the zigzag strip, above $\omega\delta_0/u_\infty = 1.6$, the noise levels are contaminated by self-noise from the bypass transition strip.

This analysis therefore suggests that a zigzag strip outperforms the staggered grid of blocks in terms of low trip self-noise.

6 CONCLUSION

To force the flow from a laminar state into a turbulent state at a specific position of interest, a boundary layer transition trip is generally used. During more recent applications, transition strips were used to match transition locations and boundary layer growth so that similar trailing edge flow characteristics were obtained when comparing, e.g., airfoil noise simulations with acoustical experiments.

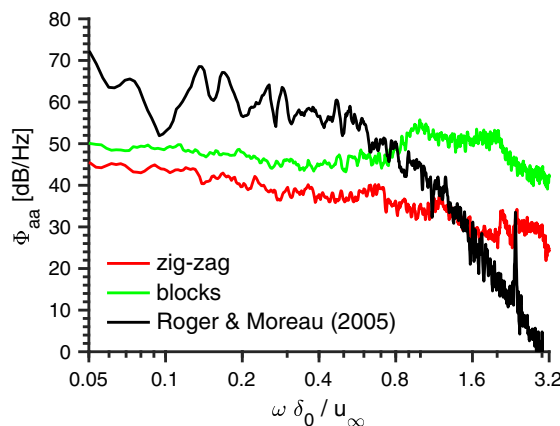


Fig. 14—Noise levels at a distance of 0.11 above the center of the trip.

Though the flow topology arising from the so-called bypass transition process is extensively addressed in the past, several issues are left open. The motivation for the current research is to understand the properties of simulated transition strips for future aeroacoustic simulations. A staggered grid of cubic blocks for transition was analyzed and compared with a more conventional, zigzag strip using flow results from the Lattice Boltzmann relation.

The velocity and pressure field was used to quantitatively visualize the flow topology field around both tripping devices. The trips were shown to be successful to enforce transition, but the observed transition scenario suggests that a zigzag strip is more efficient as a bypass transition process compared to the staggered grid of cubes since the spanwise vortices are undulated more effectively from the trip. This could be a result of a larger frontal area of the trip as well as a smaller wavelength of the zigzag strip. These spanwise instabilities enhance the development of a canonical fully turbulent boundary layer. Visualizations of the mean flow revealed periodic streamwise streaks behind the transition strips, with the most distinctive streaks being visible behind the staggered grid of cubes. In general, a canonical fully turbulent boundary layer was experienced after $40\delta_0$ for a zigzag strip, while the staggered grid of blocks needed at least $80\delta_0$ to convergence. This is confirmed by analyses of shape factor, vorticity and spanwise coherence. It was concluded that, in terms of aerodynamics, the zigzag strip outperforms the staggered grid of blocks.

Finally, near-field acoustics was analyzed by investigating the pressure fluctuations in its frequency domain. At high frequencies, the staggered grid of blocks adds a penalty of 20 dB self-noise on top of the zigzag strip structure, making the zigzag bypass transition more suitable for, e.g., trailing edge noise prediction.

7 ACKNOWLEDGMENTS

This research is funded and supported by Siemens Wind Power A/S, Brande, Denmark.

8 REFERENCES

1. R. van Rooij and W. Timmer, "Roughness sensitivity considerations for thick rotor blade airfoils", *Journal of Solar Energy Engineering*, **125**, 468–478, (2003).
2. A. Braslow and E. Knox, "Simplified method for the determination of critical height of distributed roughness particles for boundary layer transition at Mach numbers from 0 to 5", Technical Report, 4363, NACA TN, (1958).
3. R. Adrian, "Hairpin vortex organization in wall turbulence", *Physics of Fluids*, **19**, 041301, (2007).
4. E. Reshotko, "Transition issues for atmospheric entry", *45th IAA Aerospace Science Meeting and Exhibit*, **304**, (2007).
5. P.S. Klebanoff and K.T. Tidstrom, "Mechanism by which a two-dimensional roughness element induces boundary-layer transition", *Physics of Fluids*, **15**(7), 1173–1188, (1972).
6. M. Dalle and L. Meyer, "Turbulent convective heat transfer from rough surfaces with two-dimensional rectangular ribs", *International Journal of Heat and Mass Transfer*, **20**(6), 583–620, (1977).
7. R.J. Volino, M.P. Schultz and K.A. Flack, "Turbulence structure in a boundary layer with two-dimensional roughness", *Journal of Fluid Mechanics*, **635**, 75–101, (2009).
8. C. Lyon, M. Selig and A. Broeren, "Boundary layer trips on airfoils at low Reynolds number", *35th AIAA Aerospace Science Meeting and Exhibit*, **511**, (1997).
9. G. Elsinga and J. Westerweel, "Tomographic-PIV measurement of the flow around a zigzag boundary layer trip", *Experiments in Fluids*, **52**, 865–876, (2012).
10. L. Erm and P. Joubert, "Low-Reynolds number turbulent boundary layers", *Journal of Fluid Mechanics*, **230**, 1–44, (1991).
11. S. Leonardi, P. Orlandi, R.J. Smalley, L. Djenidi and R.A. Antonia, "Direct numerical simulations of turbulent channel flow with transverse square bars on one wall", *Journal of Fluid Mechanics*, **491**, 229–238, (2003).
12. S. Lee and H. Sung, "Direct numerical simulation of the turbulent boundary layer over a rod-roughened wall", *Journal of Fluid Mechanics*, **584**, 125–146, (2007).
13. J.H. Lee and H.J. Sung, "Very-large-scale motions in a turbulent boundary layer", *Journal of Fluid Mechanics*, **673**, 80–120, (2011).
14. P. Andersson, M. Berggren and D. Henningson, "Optimal disturbances and bypass transition in boundary layers", *Physics of Fluids*, **11**, 134–150, (1999).
15. L. Brandt, P. Schlatter and D. Henningson, "Transition in boundary layer subject to free-stream turbulence", *Journal of Fluid Mechanics*, **517**, 167–198, (2004).
16. X. Wu and P. Moin, "Direct numerical simulation of turbulence in a nominally zero-pressure gradient flat-plate boundary layer", *Journal of Fluid Mechanics*, **630**, 5–41, (2009).
17. D. Lockard, L. Luo and B.A. Singer, "Evaluation of the Lattice-Boltzmann equation solver PowerFLOW for aerodynamic applications", Technical report, NASA Reference Publication 210550, (2000).
18. A. de Jong and H. Bijl, "Airfoil sharp trailing edge aeroacoustics using a Lattice Boltzmann method", *AIAA Workshop on Benchmark problems for Airframe Noise Computations*, **1**, 103–126, (2010).
19. F. Perot, M.S. Kim, M. Meskine and D. Freed, "NREL wind turbine aerodynamics validation and noise predictions using a Lattice Boltzmann Method", *18th AIAA/CEAS Aeroacoustic Conference*, **2290**, 1–13, (2012).
20. K. Habibi, H. Gong, A. Najafi-Yarzdı and L. Mongeau, "Numerical simulations of sound radiated from internal mixing nozzles with forced mixers using the Lattice Boltzmann Method", *19th AIAA/CEAS Aeroacoustic Conference*, **2143**, 1–15, (2013).
21. M. Sanjose, C. Meon, V. Masson and S. Moreau, "Direct numerical simulation of acoustic reduction using serrated trailing-edge on an isolated airfoil", *20th AIAA/CEAS Aeroacoustics Conference*, **2324**, 1–15, (2014).
22. W.C.P. van der Velden, S. Probsting, A.H. van Zuijlen, A.T. de Jong, Y. Guan and S.C. Morris, "Numerical and experimental investigation of a beveled trailing-edge flow field and noise emission", *Journal of Sound and Vibration*, **384**, 113–129, (2016).
23. S. Succi, *The Lattice Boltzmann Equation for Fluid Dynamics and Beyond*, Oxford University Press, (2001).
24. H. Chen, S. Chen and W. Matthaeus, "Recovery of the Navier-Stokes equations using a lattice-gas Boltzmann method", *Physical Review*, **45**(8), R5339–R53342, (1992).
25. P.L. Bhatnagar, E.P. Gross and M. Krook, "A model for collision processes in gases: Small amplitude processes in charged and neutral one-component systems", *Physical Review*, **94**(3), 511–525, (1954).
26. J. Preston, "The minimum Reynolds number for a turbulent boundary layer and the selection of a transition device", *Journal of Fluid Mechanics*, **3**, 373–384, (1958).
27. J. Gibbings, "On boundary layer transition wires", Technical Report CP-462, Aeronautical Research Council, (1959).

28. F. White, *Viscous Fluid Flow*, 3rd edition. McGraw-Hill, New York, (2006).
29. M. Calaf, C. Meneveau and J. Meyers, "Large eddy simulation of fully developed wind-turbine array boundary layers", *Physics of Fluids*, **22**(015110), 1–16, (2010).
30. P. Schlatter and R. Orlu, "Assessment of direct numerical simulation data of turbulent boundary layers", *Journal of Fluid Mechanics*, **659**, 116–126, (2010).
31. S. Ghaemi and F. Scarano, "Counter-hairpin vortices in the turbulent wake of a sharp trailing edge", *Journal of Fluid Mechanics*, **689**, 317–356, (2011).
32. S.K. Robinson, "Coherent motions in the turbulent boundary layer", *Annual Review of Fluid Mechanics*, **23**(1), 601–639, (1991).
33. P.S. Klebanoff, K.T. Tidstrom and L. Sagent, "The three-dimensional nature of boundary layer instability", *Journal of Fluid Mechanics*, **12**, 1–34, (1962).
34. I. Castro and E. Epik, "Boundary layer development after a separated region", *Journal of Fluid Mechanics*, **374**, 91–116, (1998).
35. A. Alving and H. Fernholz, "Turbulence measurements around a mild separation bubble and downstream of reattachment", *Journal of Fluid Mechanics*, **322**, 297–328, (1996).
36. M. Goody, "Empirical spectral model of surface pressure fluctuations", *AIAA Journal*, **42**(9), 1788–1794, (2004).
37. S. Moreau and M. Roger, "Competing broadband noise mechanisms in low-speed axial fans", *AIAA Journal*, **45**(1), (2007).